doi.org/10.15392/2319-0612.2025.2909
Braz. J. Radiat. Sci., Rio de Janeiro
2025, 13(3A) | 01-22 | e2909
Editor: Prof. Dr. Bernardo Maranhão Dantas
Editor: Prof. Dr. Ademir Amaral
Submitted: 2025-04-28
Accepted: 2025-09-10

Use of Lymphoscintigraphy Images in Nuclear Medicine to Obtain the Distribution of ^{99m}Tc Photons in Computational Exposure Models

Lins[a*], J.A.G.; Vieira[b], J.W.; Lima[a], F.R.A.; Farias[a], W.A.W.A; Silva[a], V.H.F.F.; Silva[c], J.M.; Lopes Filho[c], F.J.; Pena[b], J.M.G.; Santos[a], L.C.S.

[a]Universidade Federal de Pernambuco (UFPE), 50.740-550, Recife, Pernambuco, Brasil.
[b]Instituto Federal de Educação, Ciência e Tecnologia de Pernambuco (IFPE), 50.740-545, Recife, Pernambuco, Brasil.
[c]Centro de Medicina Nuclear de Pernambuco (CEMUPE), 52.010-140, Recife, Pernambuco, Brasil.

*Correspondence: jorgelins93@hotmail.com

Abstract: This study aims to create a source catalog for Lower Limb Lymphoscintigraphy (LLL) examinations in Nuclear Medicine, using real lymphoscintigraphy images from adult male patients. The DIP (Digital Image Processing) software, developed by the Research Group on Computational Dosimetry and Embedded Systems (GPDC&SE), was used to adjust the anteroposterior (AP) and posteroanterior (PA) medical images to the frontal section of the anthropomorphic phantom MASH_sup (Male Adult meSH in supine position). The images were summed line by line, generating a **.SGI** file, which was processed by the Monte Carlo software to produce the source catalog stored in the file MSUPLC_TC99m.txt. This file contains information for each slice, including the slice number, the area of the source points, and the value of the associated cumulative distribution function (CDF). As a result, a catalog based on real clinical data was successfully generated, which enables the replacement of generic internal sources in the Computational Exposure Models of the GPDC&SE. This makes it possible to simulate LLL examinations more realistically. In the future, this methodology may be extended to female patients, different phantoms, and other scintigraphic procedures. This work represents an advancement in computational dosimetry and personalized nuclear medicine, as it enables simulations that more accurately reflect patient-specific anatomical and physiological characteristics.

Keywords: Nuclear Medicine, Lymphoscintigraphy, Image Processing, Computer-Assisted, Computer Simulation.

BJRS
BRAZILIAN JOURNAL OF RADIATION SCIENCES

doi.org/10.15392/2319-0612.2025.2909
Braz. J. Radiat. Sci., Rio de Janeiro
2025, 13(3A) | 01-22 | e2909
Editor: Prof. Dr. Bernardo Maranhão Dantas
Editor: Prof. Dr. Ademir Amaral
Submitted: 2025-04-28
Accepted: 2025-09-10

Uso de Imagens de Linfocintilografia em Medicina Nuclear para Obter a Distribuição de Fótons de ^{99m}Tc em Modelos Computacionais de Exposição

Resumo: Este estudo tem como objetivo criar um catálogo de fontes para exames de Linfocintilografia de Membros Inferiores (MMII) em Medicina Nuclear, utilizando imagens reais de linfocintilografia de pacientes adultos do sexo masculino. O software DIP (Processamento Digital de Imagens), desenvolvido pelo Grupo de Pesquisa em Dosimetria Computacional e Sistemas Embarcados (GPDC&SE), foi utilizado para ajustar as imagens médicas anteroposteriores (AP) e posteroanteriores (PA) à seção frontal do fantoma antropomórfico MASH_sup (Male Adult meSH in supine position). As imagens foram somadas linha por linha, gerando um arquivo **.SGI**, o qual foi processado pelo software de Monte Carlo para produzir o catálogo de fontes armazenado no arquivo MSUPLC_TC99m.txt. Este arquivo contém informações para cada fatia, incluindo o número da fatia, a área dos pontos-fonte e o valor da função de distribuição acumulada (FDA) associada. Como resultado, foi gerado com sucesso um catálogo baseado em dados clínicos reais, que possibilita a substituição das fontes internas genéricas nos Modelos Computacionais de Exposição do GPDC&SE, permitindo simulações mais realistas dos exames de MMII. Futuramente, espera-se aplicar essa metodologia a pacientes do sexo feminino, outros tipos de fantomas e diferentes exames cintilográficos. Isso representa um avanço na dosimetria computacional e na medicina nuclear personalizada, permitindo simulações mais fiéis às características anatômicas e fisiológicas dos pacientes

Palavras-chave: Medicina Nuclear, Linfocintilografia, Processamento Digital de Imagens, Simulação por Computador.

1. INTRODUCTION

Nuclear Medicine is a medical specialty that employs safe, virtually painless, and non-invasive methods using radioactive materials for diagnostic and therapeutic purposes. These radioactive materials are used in minimal quantities and combined with pharmaceuticals, resulting in compounds known as radiopharmaceuticals (RP) [1]. Unlike conventional radiological imaging, which primarily focuses on anatomical structures, Nuclear Medicine uses RPs to assess the physiological function of organs and living tissues, enabling imaging, diagnosis, and treatment.

Radiopharmaceuticals consist of a radionuclide, which allows for external detection, and a biologically active molecule or pharmaceutical that acts as a carrier, determining localization and biodistribution. In some radiopharmaceuticals (e.g., iodine, gallium, and thallium), the radioactive atom itself provides the desired targeting properties. Radiopharmaceuticals may also be referred to as radiochemicals or radiotracers; the latter term emphasizes their administration in subpharmacological doses that "trace" a specific physiological or pathological process in the body [2]. The resulting images are referred to as scintigraphic images, as the detector material of the gamma camera (the imaging device used in scintigraphy) is composed of scintillating crystals.

There are various procedures in Nuclear Medicine, such as bone, renal, and thyroid scintigraphy, each applied to different body regions [3]. Additionally, lymphoscintigraphy (LC) of the upper and lower limbs, also using Tc-99m, is included in this context. LC is an essential procedure for evaluating the lymphatic system, performed by injecting a particulate radiotracer into the soft tissue of the studied region, followed by image acquisition to assess the lymphatic system and lymph nodes [4]. Several aspects of this procedure — including

the type of radiotracer used, injection site, and image acquisition timing — may vary across institutions, with protocols adapted to logistical and local specificities.

Lymphedema is a condition affecting millions worldwide, with causes ranging from parasitic infections to complications from vascular surgeries and cancer treatments [5]. LC plays a key role in diagnosis by distinguishing lymphedema from other causes of edema, such as venous insufficiency or obesity [3]. Early diagnosis and proper treatment can prevent complications, such as skin changes, recurrent infections, and functional limitations. The lower limbs are among the most commonly affected regions [6]. Lymphoscintigraphy is particularly valuable not only for confirming lymphatic dysfunction but also for guiding therapeutic decisions, especially when clinical findings are inconclusive or when surgical interventions are being considered [7].

Digital processing of medical images enables the manipulation and analysis of real data obtained from various imaging modalities. These techniques are essential for preparing and refining clinical images, allowing the development of personalized models and the construction of anatomical scenarios for future simulations and studies in the field of Medical Physics. Computational methodologies that utilize medical images yield more realistic and accurate results for assessing patient dose distributions [8].

This integration of real clinical distributions (derived from patient images) into a source catalog spatially adapted to an anthropomorphic phantom represents a methodological advance toward more realistic and individualized simulations in Nuclear Medicine.

Extensive research has been conducted to improve image quality and develop innovative imaging modalities. The information and accuracy provided by medical images are fundamental to clinical decision-making. Computational modeling offers a safe and efficient means to generate realistic data and enhance the understanding of radiation physics. These approaches are valuable tools for advancing research and development in medical imaging [9].

For computational dosimetry, Computational Exposure Models (CEMs) are employed. These models are broadly defined as anthropomorphic simulators (phantoms) coupled with radiation transport codes that use algorithms for radioactive sources [10, 11]. Several dosimetric studies using CEMs have been and continue to be developed by researchers from the Numerical Dosimetry Group (GDN) and the Research Group on Computational Dosimetry and Embedded Systems (GPDC&SE), with information available at: http://dosimetrianumerica.org/.

Computational anthropomorphic phantoms are valuable tools for calculating absorbed or equivalent doses in radiosensitive organs and tissues of the human body [12]. For this study, the MASH_sup phantom (Male Adult meSH in the supine position) was selected due to its lying position and the presence of several source organs. The primary organs of interest were the lymph nodes and liver, corresponding to those observed in lymphoscintigraphy images collected from adult male patients.

Accordingly, this study proposes the adaptation of lower limb lymphoscintigraphy images from adult male patients to the MASH_sup phantom, with segmentation of the lymph nodes and liver to generate a three-dimensional source model. Based on this model, a source catalog was developed for application in computational simulations.

2. MATERIALS AND METHODS

The first stage of this study involved the use of Nuclear Medicine images, specifically Lymphoscintigraphy of the Lower Limbs (LLL), obtained from three adult male patients. These patients did not present clinical signs of lymphatic disorders, such as lower limb lymphedema, at the time of the examination. The use of male patients was due to their availability during the image acquisition period and is part of the initial phase of a broader project that also includes female subjects. The images were acquired at a Nuclear Medicine

clinic in Recife and consisted of whole-body scans in both anterior-posterior (AP) and posterior-anterior (PA) projections. The images were taken in both the early phase (immediately after the radiopharmaceutical injection) and the late phase (one hour after the injection), as shown in Figure 1.

This study was approved by the Research Ethics Committee of the Universidade Federal de Pernambuco (Ethics Approval Registration Number: 80579824.3.0000.5208, Opinion Number: 6.954.967), in accordance with all applicable ethical guidelines, ensuring patient data confidentiality and privacy.

The computational work was carried out in the Numerical Dosimetry Laboratory (LDN) at the Instituto Federal de Educação, Ciência e Tecnologia de Pernambuco (IFPE), Recife Campus, using computers with an Intel Core i7 X990 @3.47GHz processor, 24 GB of RAM, and a 64-bit Windows 7 Ultimate operating system. The anthropomorphic phantom MASH_sup, in **.SGI** format, was used to simulate the necessary anatomical conditions for the study.

Image processing and data analysis were performed using the DIP (Digital Image Processing) software [13], developed by GPDC&SE, and the MonteCarlo software, which initially had a version [14] and was later organized into a consolidated version [15-17]. This was used to create the file MSUPLC_TC99m.txt, containing the parameters (Slice, AreaXY, CDF – Cumulative Distribution Function) of the MASH-SUP phantom. In addition, the ImageJ (Fiji) software was employed for medical image data analysis, and Paint (Microsoft Paint™) was used for visual adjustments, including color modifications, such as changing black to white, to enhance the visibility of areas of interest.

Figure 1: Patient A: Two early scans (left); two late scans (1 hour) (right)

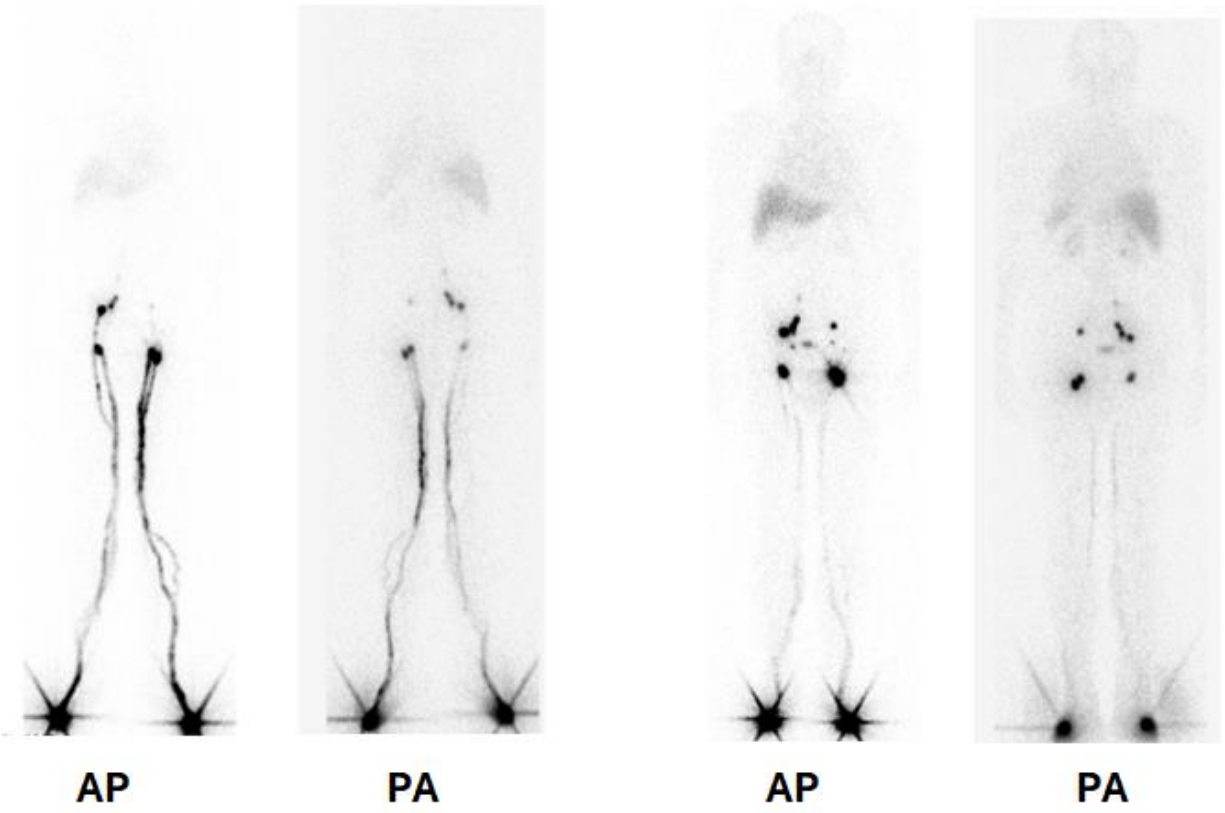

2.1. Visual Adjustment with Microsoft Paint™ Software

The first step in image processing involved using Microsoft Paint™ software to perform initial adjustments to the medical images. The "Invert Colors" tool was used to adjust the contrast of the images, enabling more precise and more accurate visualization of the areas of interest.

This process was carried out to ensure that the images had a consistent visual appearance suitable for the subsequent processing steps. Visual standardization was crucial for maintaining uniformity across the images of all patients, including the three male patients (A, B, and C), thereby ensuring the quality of the data for subsequent steps. Figure 2 illustrates the result for male patient A, representing the final visualization before the following processing steps.

It is worth noting that this visual adjustment was performed solely using Microsoft Paint™, but the same adjustment could have been achieved using other software tools, such as DIP, which was employed in subsequent processing stages.

Figure 2: Invert Colors – Patient A: Early scan

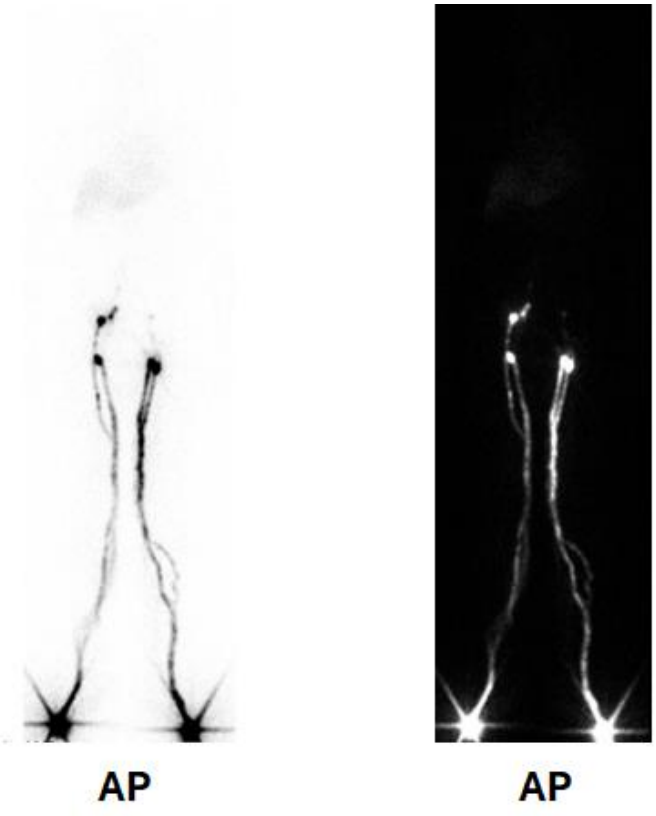

2.2. Image and Data Processing with DIP Software

The second stage involved the use of the DIP software. The images, which now had the background adjusted, were processed in several steps to ensure that their dimensions and alignment matched those of the MASH_sup anthropomorphic phantom, as well as adjustments to the phantom itself.

2.2.1. Dimension Adjustment (Y Height and X Base):

The first adjustment made to the images was in height (Y-axis), without distorting the aspect ratio. The width (base, X-axis) was adjusted later by adding and trimming borders to ensure that the center of the patient images aligned with the anatomical center of the phantom. This adjustment was made for both the AP (anteroposterior) and PA (posterior-anterior) scans, and varied for each of the three patients (A, B, and C) due to individual anatomical differences. Both the early phase (immediately after the radiopharmaceutical injection) and the late phase (1 hour later) also required specific adjustments for each image (Figure 3).

Figure 3: Use of DIP software – Image Centering

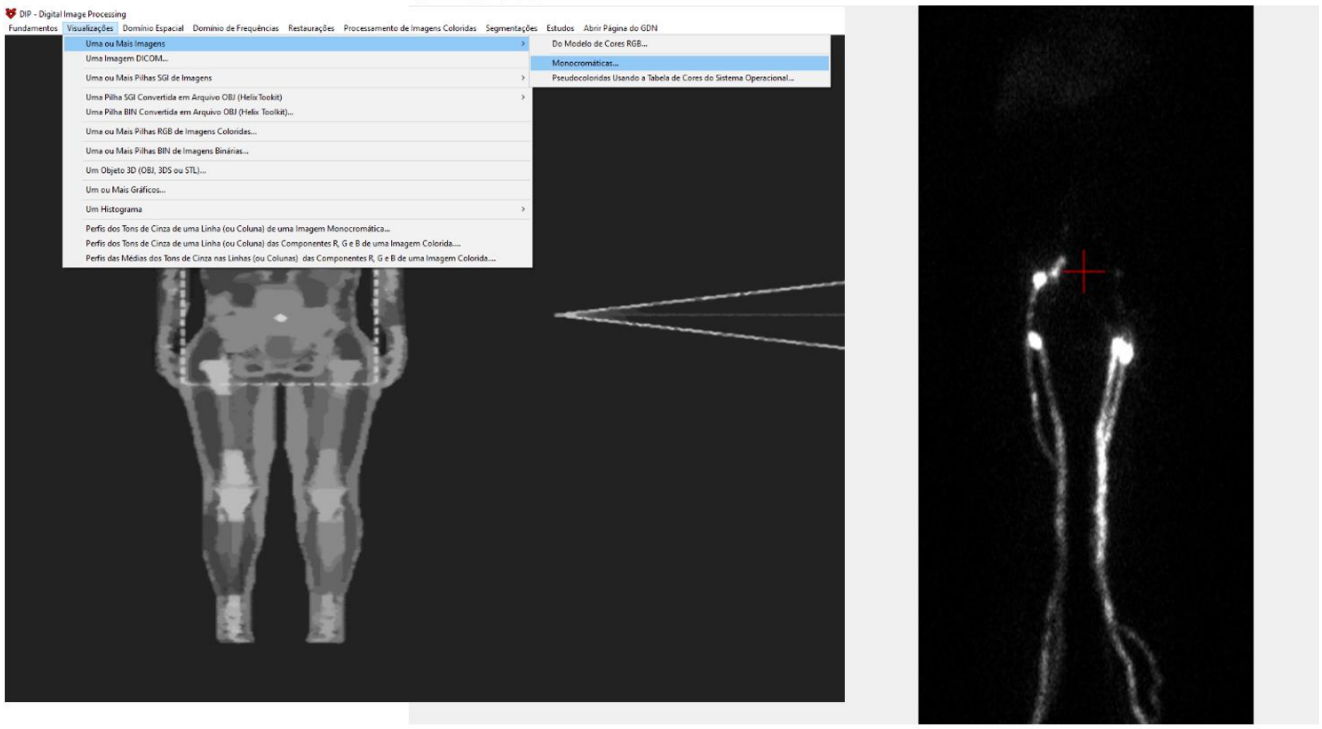

2.2.2. Adjustment of MASH_sup Phantom:

After adjusting the patient images, the phantoms were adjusted accordingly. This process involved changing the tissue IDs of the phantoms, keeping only the IDs for the lymph nodes and liver, which were the organs of interest in the patient images (Figure 4). For this, a pre-defined list of IDs, already established by GPDC&SE for the male phantom,

was used (Table 1). Table 1 presents a summary of some of the IDs found in the MASH_sup phantom. Since there are hundreds of distinct IDs, the table includes only a representative selection of these values.

Figure 4: Comparison of the MASH_sup phantom with all organs (a); and with only the liver and lymph node IDs (b) for the same slice – DIP software visualization.

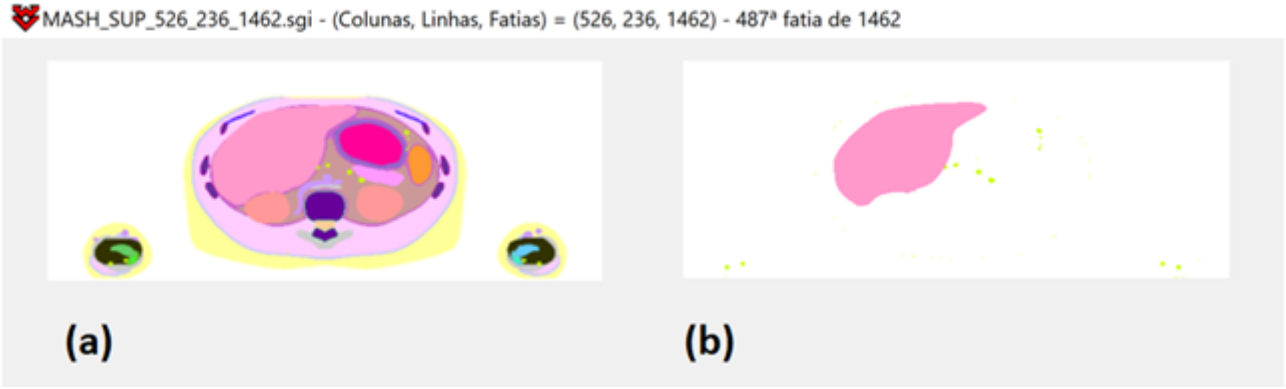

Table 1 : List of some IDs that can be found in the MASH_sup phantom

ID	Structure Name
0	Vacuum
1	Skin
2	Fat
4	Eyes
5	Eye lenses
6	Muscle
13	Liver
39	Prostate
40	Testes
41	Lymph nodes
184	Left femur – Lower Spongy Tissue
186	Right femur – Lower Spongy Tissue
200	Internal air

2.2.3. Creation of the frontal projection of the phantoms:

A frontal projection in .png format was generated, representing the phantom, including lymph nodes and liver, from a coronal slice. This image (Figure 5) was used as an

'anatomical base' to overlay the patient images through multiplication operations, explained later. For the cases where the patient images were in posteroanterior (PA) view, it was necessary to rotate the phantoms 180° around the Z-axis, using the DIP software, so that the anatomical orientation between the phantoms and the PA images would be compatible.

Figure 5: Frontal projection of the phantom

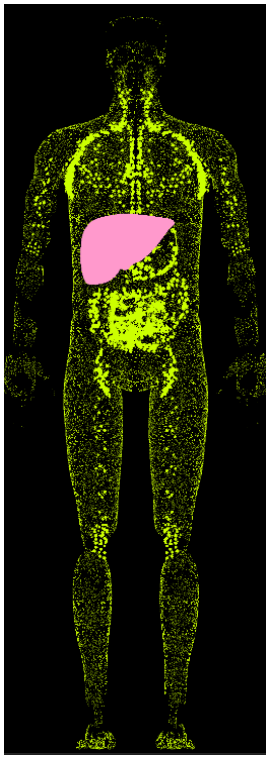

2.2.4. Change of intensity values (IDs) in the frontal projection:

To prepare the phantom image for integration with the patient images, a binary logical mask was created using the ID swap tool in the DIP software. Initially, the frontal projection of the phantom, obtained from the coronal cut, was colored and showed different intensities associated with the anatomical structures represented by the original IDs (Liver: 13; Lymph Nodes: 41).

The pixels with IDs 13 and 41 were kept as "true" (1), while the others were converted to "false" (0), resulting in a 2D binary mask – referred to as the "2D Phantom Mask." The resulting image appears darkened, as shown in Figure 6 (a), because the intensity values were

standardized to 1 in the pixels of interest and 0 in the background. This standardization is essential for the subsequent processing, where the patient image will be multiplied by this mask. Figure 6 (b) shows the same image in a more illustrative way with the application of a color palette to facilitate the visualization of the regions marked with a value of 1.

Figure 6: Comparison of Visualizations: Black and Color.

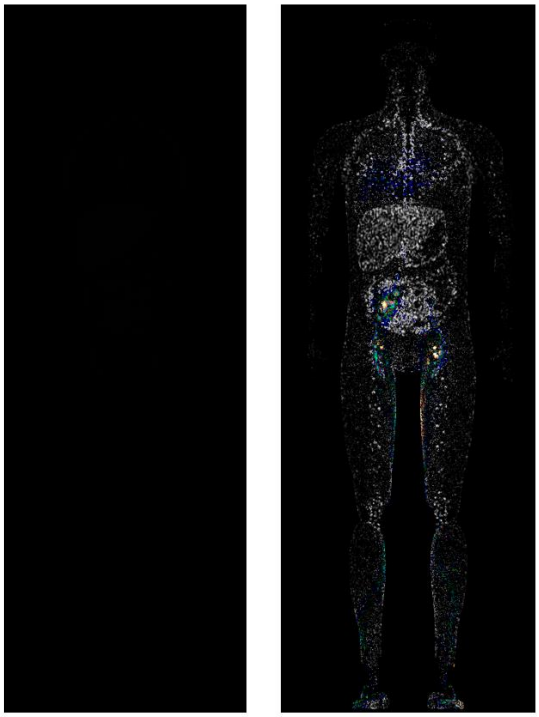

2.2.5. Image Multiplication:

After preparing the frontal projection of the MASH_sup phantom and the patient images, a pixel-by-pixel multiplication was performed between these two images using the arithmetic operations tool in the DIP software. In this process, the patient image represents the actual distribution of radioactive activity, with pixel intensities reflecting the uptake of the radiopharmaceutical in different anatomical regions. The phantom image, in turn, was converted into a binary mask, containing only the lymph nodes and liver as valid regions (value 1), with all other pixels set to 0.

The multiplication of these two images resulted in a hybrid image (Figure 7), in which only areas with value 1 in the mask retain the pixel intensities from the patient's image. This way, the clinical details of the exam are preserved exclusively in the anatomical structures of interest, such as the lymph nodes and liver, as defined in the voxelized models.

Figure 7: Example of the multiplication image: MASH_sup x Lymphoscintigraphy.

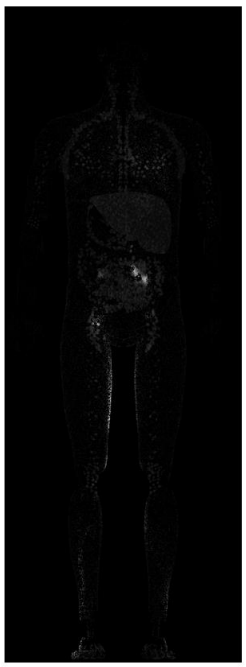

PA

2.2.6. Sum of AP and PA Images and Generation of .SGI Files:

The final step performed using the DIP software involved summing the AP and PA images of each patient with the MASH_sup phantom, generating individual **.SGI** files for each patient in both the early and late phases. This summation aimed to combine the contributions from both projections, ensuring that all radiation is integrally considered in the simulation process.

This operation was conducted line by line (2D image rows) to quantify the total intensity in each combined projection. The resulting value in each 2D image line was then associated with the corresponding slice of the 3D model. The final summed image was

converted to grayscale, with intensity values ranging from 0 to 255, representing different activity levels.

The output file naming follows the standard **MSUPLC_TC99M_X_X**, where "M" refers to the MASH_sup phantom, "LC" to the lymphoscintigraphy exam, and "X" indicates the patient (A, B, or C) and the exam phase. Note that the original terms **"Precoce"** and **"Tardia"** (which mean **early** and **late**, respectively) are retained in the filenames, as they are part of the data source and naming convention.

Figure 8 shows the images for patient A in the **Precoce** (left) and **Tardia** (right) phases, visualized using the Volume Viewer tool in Fiji (ImageJ). Subsequently, Table 2 presents an organized summary of all steps carried out in the DIP software, from image preparation to the generation of the final files used as input for Monte Carlo simulations. The menu path is shown in Portuguese, which corresponds to the official language of the software interface.

Figure 8: MSUPLC_TC99M_A_PRECOCE (left) e MSUPLC_TC99M_A_TARDIA (right).

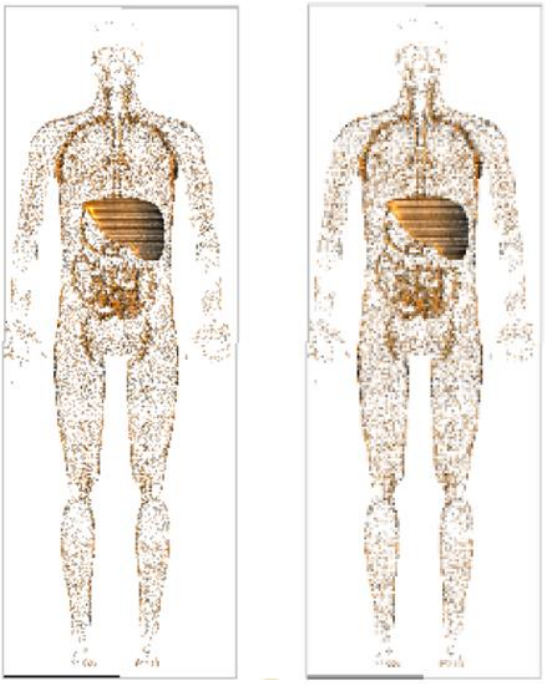

Table 2: Steps of Image and Data Processing in the DIP Software

STEPS	DESCRIPTION	MENU PATH
1	Equalization of image height with that of the phantom (Y)	Fundamentos → Mantendo o Id do Pixel (voxel de entrada) → De uma Imagem sem Deformação com Base na Altura (Y)...
1	Finding the anatomical center of the image based on its width (X)	Visualizações → Uma ou Mais Imagens → Monocromáticas...
1	Addition of border	Fundamentos → Adicionar uma Moldura (com Largura e Altura Maiores ou Iguais às da Imagem) a uma Imagem...
1	Finding the new anatomical center of the image	Visualizações → Uma ou Mais Imagens → Monocromáticas...
1	Reduction of width, aligning the center of the image with the phantom's center	Visualizações → Cortes → Área de uma Imagem → Digitando a localização e as dimensões...
2	Replacement of tissue IDs, keeping lymph nodes and liver, and replacing others with ID = 0	Fundamentos → Trocas → Em uma Pilha SGI de Imagens → Trocar → Troca Todos os Ids por um Idnovo Exceto uma Lista de Ids Fornecidos...
3	Frontal projection of the phantom with lymph nodes and liver, using ID = 0 as background, saved in .png format	Fundamentos → Projeções e Seções → Projeção Frontal → Usando id = 0 como Fundo...
3	Adjustment of phantom orientation by 180° rotation around the Z-axis to match PA images	Fundamentos → Rotações → Ortogonais de uma Pilha SGI...
4	Conversion of all grayscale tones in the phantom's frontal projection to a single identifier (ID = 1), resulting in a uniformly dark gray image.	Fundamentos → Trocas → Em uma Imagem → Trocar → Um Intervalo de Ids por um Único Id...
5	Multiplication of the phantom image with the lymphoscintigraphy image	Domínio Especial → Operações Aritméticas → Multiplicação Pixel a Pixel (Voxel a Voxel) → Duas Imagens...
6	Sum of AP and PA images, creating **.SGI** files	Estudos → Medicina → Linfocintilografia → Abrir as Imagens AP e PA, Somar os TCs por Linha, e Salvar um SGI com Fonte Especificada...

2.3. Creation of the MSUPLC_TC99m.txt Sources Catalog in the MonteCarlo Software for Use in EGSnrc Simulations

The Monte Carlo software was used to convert the final .SGI files from the DIP phantoms into structured .txt files, named MSUPLC_TC99m.txt. Each line in the file represents an axial slice of the phantom, containing the slice number, limits of the area of interest (xmin, xmax, ymin, ymax), and the value of the CDF, which replaces the standard source in the Monte Carlo simulations by reflecting the spatial distribution of the radioactive activity observed in the actual images.

From the images, the Monte Carlo software counts the non-zero voxels (indicating radioactive emission) in each 3D slice and normalizes them to generate the Probability Density Function (PDF). The CDF is obtained by accumulating the PDF, allowing probabilistic selection of the emitting slice based on a random number between 0 and 1. As an increasing function, the CDF speeds up the search for the corresponding slice, optimizing the performance of the EGSnrc code.

The MSUPLC_TC99m.txt catalog includes data from six male MCEs, considering both early and late phases of the exam for the same patients. The phantoms are numbered from 01 to 06. For example, the entry "01 1395 MSUPLC_Tc99m_PA" refers to phantom 01 with 1395 slices, corresponding to the early phase (P) of patient A, while "04 1392 MSUPLC_Tc99m_TA" represents the late phase (T) for the same patient, with 1392 slices. Thus, the catalog allows different activity distributions to be incorporated for the same individual based on the exam phase.

3. RESULTS AND DISCUSSIONS

The methodology adopted in this study was based on the use of lymphoscintigraphy images from healthy male patients, due to the availability of data compatible with the anthropomorphic models used. This choice represents a relevant limitation, as it restricts the generalization of the results to other populations, such as female patients or individuals with anatomical changes resulting from lymphatic diseases. It should be emphasized that, due to limitations of the MASH_sup model, structures such as lymphatic vessels in the lower limbs are not represented, which may restrict the presence of activity in certain regions after the multiplication process, as observed in Figure 7.

The MSUPLC_TC99m.txt sources catalog was successfully generated from the conversion of the images adjusted in DIP, organizing six datasets of male CEMs corresponding to different phases of the examination (early and late). Each entry in the file contains information about the total number of slices, the boundaries of the area of interest per slice, and the values of the CDF, which guide the probabilistic selection of the emitting slice during the simulation.

As an additional step, a simulation was performed using the EGSnrc code to validate the functionality of the catalog. The process required specific adjustments to the source code to ensure compatibility between the processed data and the simulator's structure. Figure 9 shows the successful compilation of the CEM MSUPLC_P_C, demonstrating that the sources catalog works correctly and that any of the source phantoms numbered from 1 to 6 can be selected as desired.

Figure 9: Interface do EGSnrc: Compilação bem-sucedida do MCE MSUPLC_P_C.

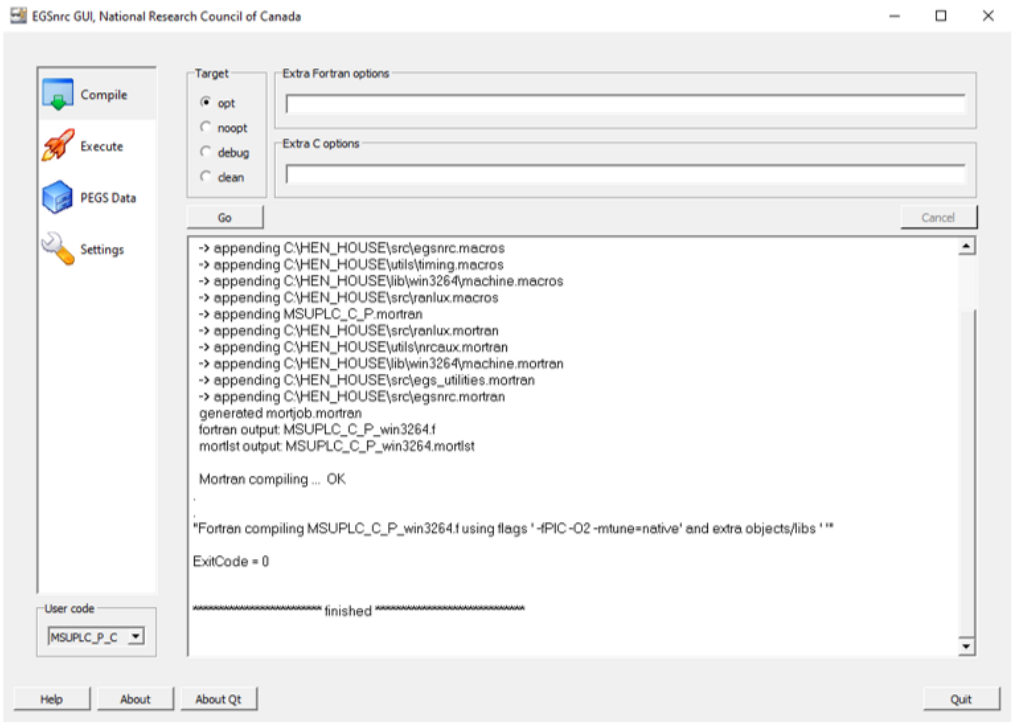

The simulations generated output files in the .data format, as shown in Figure 10. This figure displays part of the obtained results, highlighting relevant information present in the header of the files, such as "SPECTRUM Nº 3," indicating that the simulation was performed for phantom number 3 from the sources catalog (line 13), the **MSUPLC_Tc99m_PC**, and "NUMBER OF EMITTED PARTICLES: 200000000," which corresponds to the number of histories selected (line 16)

Figure 10: Results of the post-simulation output file

MSUPLC_2E8.140keV.data

```
MC-CODE/PHANTOM: EGSnrc/MASH3_supine_mic60 R0160 ICRP89/ICRU46/I
MACRO VOXEL SIZE XAL/YAL/ZAL (CM)  :   0.12    0.12    0.12
MICRO VOXEL SIZE XIL/YIL/ZIL (CM)  :   0.0060    0.0060    0.0060     RBM/3YBM SEGMENTATION AT RUNTIME
START
  DATE: 11-12-2024  TIME: 13:56:05.
STOP
  DATE: 11-12-2024  TIME: 16:58:00.
EXPOSURE CAUSED BY TC-99M DISTRIBUTED IN THE LIVER AND LYMPHATIC NODESNUMBER OF MICRO MATRICES:192 SELECTION: SYSTEMATIC   8   3   8
INTERNAL EXPOSURE, SOURCE ORGAN: LYMPHATIC NODES                                        BSC THICKNESS =  50 MICRON   ICRP MODEL
TRABECULAR BONE VOLUME FRACTION:    RIBCAGE: 0.114      SPINE: 0.113 LONG BONES: 0.152     PELVIS: 0.212 SKULL/MAND: 0.514
MAXIMUM EMITTED PARTICLE ENERGY:   140.5 keV     YIELD = 1.00     SOURCE PARTICLE :  PHOTON   NUMBER OF MEDIA:  20
CELLULARITY:  RIBCAGE= 0.600  SPINE= 0.700  LONG BONES= 0.250  PELVIS= 0.480  SKULL/MANDIBLE= 0.380
SPECTRUM NO.   3   MSUPLC_Tc99m_PC
MEAN SPECTRAL ENERGY:   0.0 keV

NUMBER OF EMITTED PARTICLES:   200000000   ECUT=    20. keV   PCUT=    2. keV   CORT=    5. keV RBM/YBM=   5. keV   TRAB=    5. keV

NO. ORGAN                       N-VOXEL     ORGAN  DOSE/CUMULAT    DOSE/EMITTED    ENER/ETOT      COEFF.OF  SPECIFIC ABSO     COEFF.OF
                                          DENSITY    ACTIVITY        PARTICLE      ABS.FRACT.     VARIANCE  RBED FRACTION     VARIANCE
                                          g/cm**3     mGy/MBq s         mGy           MEV/MEV          %          1/g             %

  1 EYES                           8748    1.0500   3.5449E-09      3.5449E-15    0.0000E+00       2.31    0.0000E+00          0.00   1
  2 ADRENALS                       7866    1.0300   8.9268E-07      8.9268E-13    0.0000E+00       0.15    0.0000E+00          0.00   2
  3 BLADDER WALL                  27822    1.0400   1.7817E-08      1.7817E-14    0.0000E+00       0.56    0.0000E+00          0.00   3
  4 BRAIN                        799162    1.0500   2.0706E-09      2.0706E-15    0.0000E+00       0.38    0.0000E+00          0.00   4
  5 ORAL MUCOSA                   40234    1.0500   1.8344E-08      1.8344E-14    0.0000E+00       0.49    0.0000E+00          0.00   5
  6 COLON WALL                   205885    1.0400   1.1799E-07      1.1799E-13    0.0000E+00       0.08    0.0000E+00          0.00   6
  7 BREASTS, GLANDULAR             5674    1.0200   1.8408E-07      1.8408E-13    0.0000E+00       0.38    0.0000E+00          0.00   7
  8 KIDNEYS                      170855    1.0500   6.1422E-07      6.1422E-13    0.0000E+00       0.04    0.0000E+00          0.00   8
  9 LIVER                        992063    1.0500   2.1139E-06      2.1139E-12    0.0000E+00       0.01    0.0000E+00          0.00   9
 10 LUNGS                       2554417    0.2800   2.6008E-07      2.6008E-13    0.0000E+00       0.03    0.0000E+00          0.00  10
 11 MUSCLE                     15982216    1.0500   7.8098E-08      7.8098E-14    0.0000E+00       0.01    0.0000E+00          0.00  11
 12 OESOPHAGUS                    22473    1.0300   3.3059E-07      3.3059E-13    0.0000E+00       0.15    0.0000E+00          0.00  12
 13 TESTES                        19470    1.0400   2.4595E-09      2.4595E-15    0.0000E+00       1.81    0.0000E+00          0.00  13
 14 PANCREAS                      77160    1.0500   5.6776E-07      5.6776E-13    0.0000E+00       0.07    0.0000E+00          0.00  14
 15 SOFT TISSUE(NOT PART OF E)  4780679    1.0400   1.4134E-07      1.4134E-13    0.0000E+00       0.02    0.0000E+00          0.00  15
 16 SMALL INTESTINE WALL         361690    1.0400   1.2123E-07      1.2123E-13    0.0000E+00       0.06    0.0000E+00          0.00  16
 17 SKIN                        1752719    1.0900   3.9456E-08      3.9456E-14    0.0000E+00       0.05    0.0000E+00          0.00  17
 18 SPLEEN                        83504    1.0400   2.9713E-07      2.9713E-13    0.0000E+00       0.09    0.0000E+00          0.00  18
 19 STOMACH WALL                  83468    1.0400   8.0067E-07      8.0067E-13    0.0000E+00       0.05    0.0000E+00          0.00  19
 20 SALIVARY GLANDS               47756    1.0300   1.3905E-08      1.3905E-14    0.0000E+00       0.50    0.0000E+00          0.00  20
 21 THYMUS                        14046    1.0300   2.0526E-07      2.0526E-13    0.0000E+00       0.24    0.0000E+00          0.00  21
 22 THYROID                       11129    1.0400   4.7362E-08      4.7362E-14    0.0000E+00       0.55    0.0000E+00          0.00  22
 23 EXTRATHORARCIC AIRWAYS        60710    1.0300   1.2021E-08      1.2021E-14    0.0000E+00       0.48    0.0000E+00          0.00  23
 24 PROSTATE                       9551    1.0300   8.0314E-09      8.0314E-15    0.0000E+00       1.44    0.0000E+00          0.00  24
 25 ADIPOSE TISSUE              8846676    0.9500   7.4067E-08      7.4067E-14    0.0000E+00       0.02    0.0000E+00          0.00  25
 26 HEART WALL                   181878    1.0500   4.0483E-07      4.0483E-13    0.0000E+00       0.05    0.0000E+00          0.00  26
 27 LYMPHATIC NODES              202182    1.0300   1.4764E-07      1.4764E-13    0.0000E+00       0.07    0.0000E+00          0.00  27
 28 GALL BLADDER WALL              5618    1.0300   8.7324E-07      8.7324E-13    0.0000E+00       0.18    0.0000E+00          0.00  28
 29 SKELETON AVERAGE            4199423    1.3700   9.9619E-08      9.9619E-14    0.0000E+00       0.02    0.0000E+00          0.00  29
 30 CORTICAL BONE TOTAL         1291630    1.9200   1.1429E-07      1.1429E-13    0.0000E+00       0.03    0.0000E+00          0.00  30
```

4. CONCLUSIONS

A methodology for constructing a catalog of sources based on real lymphoscintigraphy images of lower limbs was presented, resulting in files compatible with the EGSnrc simulator. This approach enables the representation of spatial activity distributions for different exam phases in a standardized format. The development of such catalogs based on patient-specific data represents a significant advancement in computational dosimetry by providing more accurate input for dose calculations tailored to individual anatomical and physiological conditions. This work contributes to the progress of personalized nuclear medicine, improving the precision of diagnostic and therapeutic procedures. In the future, this strategy can be extended to the development of new catalogs involving more detailed phantoms,

female patients, and other scintigraphic exams, broadening its applicability in Nuclear Medicine research and practice.

ACKNOWLEDGMENT

The authors thank the Research Group on Computational Dosimetry and Embedded Systems (GPDC&SE) for the technical support provided in the Numerical Dosimetry Laboratory at Instituto Federal de Educação, Ciência e Tecnologia de Pernambuco (IFPE) – Recife Campus.

FUNDING

This work was financially supported by the Fundação de Amparo à Ciência e Tecnologia de Pernambuco (FACEPE) through a scholarship granted to the first author.

CONFLICT OF INTEREST

We have no conflicts of interest to disclose.

All authors declare that they have no conflicts of interest.

REFERENCES

[1] Sociedade Brasileira de Física Médica. CONHEÇA A MEDICINA NUCLEAR. 2021. Disponível em: https://sbmn.org.br/comunicacao/conheca-a-medicina-nuclear/. Acessed on: 28 jun. 2021.

[2] ZIESSMAN, H. A.; O'MALLEY, J. P.; THRALL, J. H.; FAHEY, F. H. **Medicina nuclear.** Tradução Silvia Mariangela Spada. 4. ed. Rio de Janeiro: Elsevier, 2015.

[3] HIRONAKA, F. H.; SAPIENZA, M. T.; ONO, C. R.; LIMA, M. S.; BUCHPIGUEL, C. A. **Medicina Nuclear: princípios e aplicações.** São Paulo: Atheneu, 2012.

[4] SADEGHI, R.; KAZEMZADEH, G.; KESHTGAR, M. Diagnostic application of lymphoscintigraphy in the management of lymphoedema. **Hell J Nucl Med,** v. 13, n. 1, p. 6-10, 2010.

[5] SZUBA, A.; SHIN, W. S.; STRAUSS, H. W.; ROCKSON, S. The third circulation: radionuclide lymphoscintigraphy in the evaluation of lymphedema. **Journal of Nuclear Medicine,** v. 44, n. 1, p. 43-57, 2003.

[6] BARRAL, C. M.; STEHLING, A. P.; SILVA, A. C. M.; CASTRO, A. C.; IVO, C. S.; KORMAN, D. E.; MAGALHÃES, L. N.; CARVALHO, L. A.; FÉLIX, M. T. M.; MACHADO, F. S. Linfocintilografia de membros inferiores: estudo retrospectivo de 154 casos no período de março de 2009 a junho de 2010. *Revista Médica de Minas Gerais*, **v. 23**, **n. 2**, p. 182–192, 2013.

[7] DONOHOE, K. J.; CARROLL, B. J.; CHUNG, D. K. V.; DIBBLE, E. H.; DIEGO, E.; GIAMMARILE, F.; GRANT, F. D.; LAI, S. Y.; LINDEN, H.; MILLER, M. E.; PANDIT-TASKAR, N.; TAWA, N. E. Jr.; VIDAL-SICART, S. Summary: Appropriate Use Criteria for Lymphoscintigraphy in Sentinel Node Mapping and Lymphedema/Lipedema. **Journal of Nuclear Medicine**, v. 64, n. 4, p. 525–528, abr. 2023. DOI: 10.2967/jnumed.123.265560.

[8] ABOIA, L. S.; MENEZES, A. F.; CARDOSO, M. A. C.; ROSA, L. A. R. da; BATISTA, D. V. S.; CARDOSO, S. C.; SILVA, A. X.; FACURE, A. Application of digital image processing for the generation of voxels phantoms for Monte Carlo simulation. **Applied Radiation and Isotopes**, v. 70, n. 1, p. 144–148, 2012. DOI: 10.1016/j.apradiso.2011.08.017.

[9] LEE, H. Monte Carlo methods for medical imaging research. **Biomedical Engineering Letters**, v. 14, p. 1195–1205, 2024. DOI: 10.1007/s13534-024-00423-x

[10] VIEIRA, J. W. Construção de Um Modelo Computacional de Exposição para Cálculos dosimétricos Utilizando o Código EGS4 e Fantomas de Voxels. Tese de Doutorado, PROTEN, UFPE, Recife, Pernambuco, 2004.

[11] CABRAL, M. O. M. Desenvolvimento de Um Modelo Computacional de Exposição para Uso em Avaliações Dosimétricas em Gestantes. Dissertação de Mestrado, PROTEN, UFPE, Recife, Pernambuco, 2015.

[12] CASSOLA, V. F. Desenvolvimento de fantomas humanos computacionais usando malhas poligonais em função da postura, massa e altura. Tese de Doutorado, PROTEN, UFPE, Recife, Pernambuco, 2011.

[13] VIEIRA, J. W.; LIMA, F. R. A. A software to digital image processing to be used in the voxel phantom development. **Cell and Molecular Biology,** 2009, v. 3, p. 16-22. doi: 10.1170/T869.

[14] VIEIRA, J. W. Uso de Técnicas Monte Carlo para Determinação de Curvas de Isodose em Braquiterapia. Dissertação de Mestrado, PROTEN, UFPE, Recife, Pernambuco, 2001.

[15] VIEIRA, J. W.; LEAL NETO, V.; LIMA FILHO, J. M.; LIMA, L. F.; LOPES FILHO, F. J.; ROCHA, E. A.; LIMA, F. R. A. Estimate of dose distribution in voxel phantom irradiated by a planar source modeled by translational normal probability density functions. In: 2012 **International Symposium on Radiation Physics,** Rio de Janeiro, 2012.

[16] VIEIRA, J. W.; LEAL NETO, V.; LIMA FILHO, J. M.; LIMA, L. F.; LIMA, F. R. A. Modelagem Monte Carlo de regiões dos ossos trabeculares de adultos para uso em modelos computacionais de exposição. In: **Terceiro Congresso de Proteção Contra Radiações da Comunidade dos Países de Língua Portuguesa,** Lisboa, 2012.

[17] VIEIRA, J. W.; LEAL NETO, V.; LIMA FILHO, J. M.; LIMA, F. R. A. Transformation of the normal distribution for Monte Carlo modeling of regions of adult trabecular bones for use in computational models of exposure. In: 13th **International Congress of the International Radiation Protection Association,** Glasgow, 2012.

LICENSE